Supplementary Information (SI) for Physical Chemistry Chemical Physics.
This journal is © the Owner Societies 2026

# Supporting Information for

# Selective Decarboxylative Dimerization Enabled by Supramolecular Template on Ag(111)

Haiwei Wang[1], Xianfei Xu[2], Zhaokun Wang[3], Suya Dai[1], Xiang Zhang[1], Zhe Huang[1], Yongjie Chen[1], Yucheng Song[1], Cunfeng Zheng[1], Zengfu Ou[4], Yi Ji[5], Zeying Cai[6], Hongbing Ji[1], Jin Li[1,*], Zechao Yang[2,*] and Shenwei Chen[1,*]

[1] State Key Laboratory of Green Chemical Synthesis and Conversion, College of Chemical Engineering, Zhejiang University of Technology, Hangzhou, Zhejiang, CN 310014

[2] School of Physics, Hangzhou Normal University, Hangzhou, Zhejiang, CN311121

[3] School of Chemistry and Chemical Engineering, Guangxi University, Nanning, Guangxi, CN 530004

[4] College of Physics and Electronic Information Engineering, Guilin University of Technology, Guilin, Guangxi, CN 541004

[5] Institute of Functional Nano & Soft Materials (FUNSOM), Jiangsu Key Laboratory for CarbonBased Functional Materials & Devices, Soochow University, Suzhou, Jiangsu, CN 215123

[6] Spallation Neutron Source Science Center, Dongguan, Guangdong, CN 523803

**Corresponding Authors:** J. L. (lijin@zjut.edu.cn); Z. Y. (yangzechao@hznu.edu.cn); S. C. (csw@zjut.edu.cn).

# Content

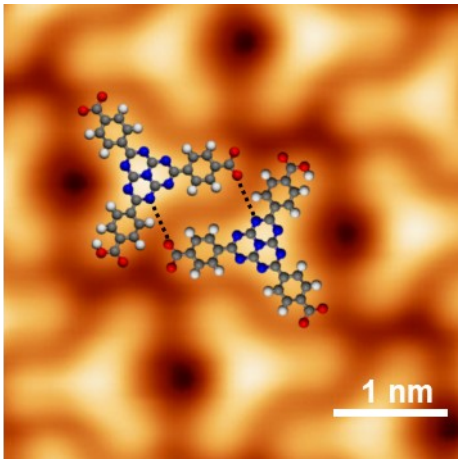


**Figure S1.** N···H–O hydrogen bonding between the HTBA core nitrogen and a protonated carboxylic acid was excluded as an alternative interaction. Tunneling parameters: $V_s$ = ⁻ 2.0 V, $I_t$ = 100 pA.

In the structure observed after annealing to 150°C, the intermolecular connectivity at the ribbon edges is characterized by a shoulder-to-shoulder configuration (Type II). Based on high-resolution STM images, the measured distance between the aromatic C–H group and the adjacent carboxylate oxygen (2.4 Å) falls within the range commonly reported for ionic hydrogen bonding interactions (C–H···O=C) on Ag(111). In contrast, as shown in Figure S1, the distance between the nitrogen atom of the HTBA core and the oxygen atom of a protonated carboxylic acid group (~4.5 Å) is significantly larger than typical N···H–O hydrogen bonding distances (small than 3 Å), making such an interaction geometrically unfavorable in the experimentally observed configuration.

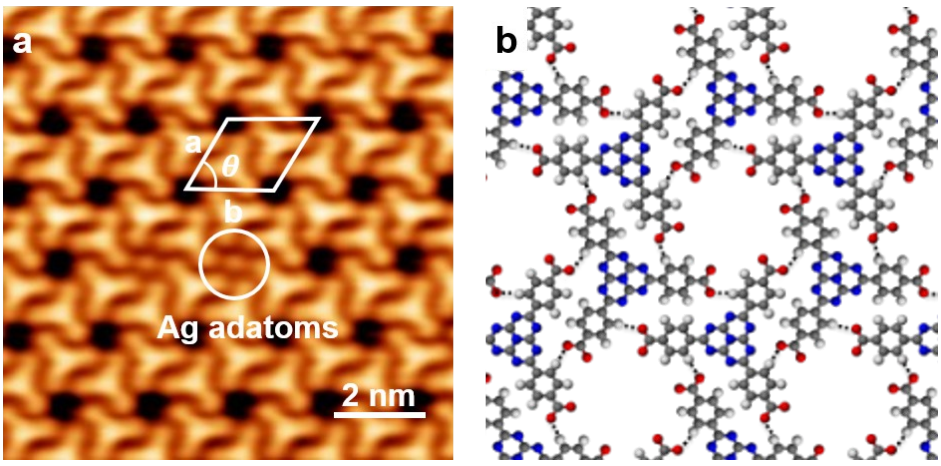


**Figure S2.** STM image and corresponding structural model of the pinwheel phase. (a) STM image of the pinwheel phase formed by HTBA molecules on Ag(111) after annealing at 150 ℃ and subsequent imaging at 78 K, with the parameters of the unit cell is measured to be $a = b = 2.0 \pm 0.05$ nm, and $\theta = 60° \pm 1°$. (b) Structual model of the pinwheel phase. Tunneling parameters: $V_s = -2.0$ V, $I_t = 100$ pA.

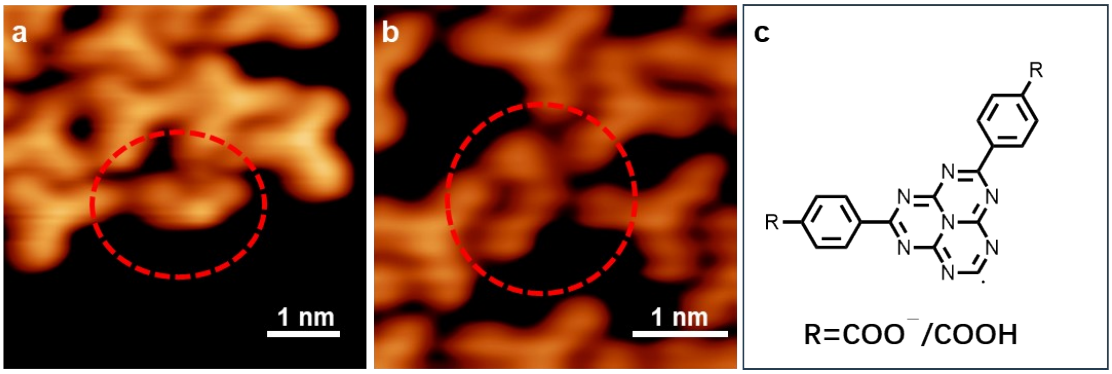


**Figure S3.** (a, b) STM images of HTBA-derived fragments on Ag(111) after annealing at ~150 °C, corresponding to molecular residues remaining after cleavage and loss of benzoic acid groups. (c) Structural model of the HTBA-derived fragment. Tunneling parameters: (a) $V_s = -2.0$ V, $I_t = 100$ pA. (b) $V_s = -2.7$ V, $I_t = 300$ pA.

Upon annealing at about 150 ℃, HTBA molecules were observed to undergo cleavage of their benzoic acid groups, yielding HTBA fragments. Although only a small number of molecules were involved in this process, it elucidates the subsequent formation of

short *d*-dimers. These dimers result from the dimerization of the HTBA fragments following the removal of the benzoic acid groups. Notably, no stable benzoic acid (BA) fragments were identified in the STM images under the present experimental conditions. This absence suggests that the BA fragments generated during the cleavage process are weakly bound and are therefore likely to desorb from the Ag(111) surface at the elevated temperatures required for annealing, rather than remaining immobilized on the surface and detectable by STM.

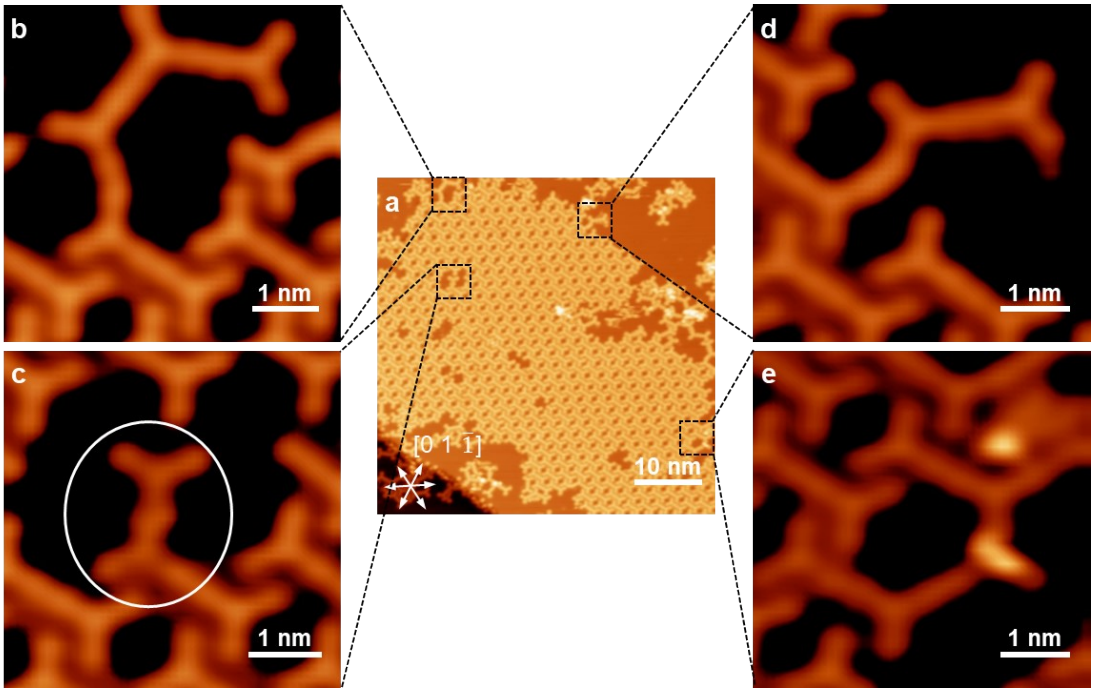


**Figure S4. STM images of rare higher-order coupling events beyond *d*-dimer formation.** (a) Large-scale and (b-e) zoomed-in STM images of the higher-order coupling products. Tunneling parameters: (a-e) $V_s = -1.6$ V, $I_t = 80$ pA.

At the edge and defect sites of the *d*-dimer domain, a small quantity of trimer and higher-order structures emerged as by-products. This phenomenon is attributed to the weakening of the molecular template effect, which left the carboxylic acid sites of the HTBA molecules unprotected and thus susceptible to dimerization reactions. Figs. S4b, S4d, and S4e display the STM images of these by-products at the edges of the *d*-dimer self-assembly domain. Additionally, Fig. S4c specifically presents the STM image of

the by-product at the defect site of the *d*-dimer self-assembled domain. The white circle denotes the short *d*-dimer, which will be discussed in detail later.

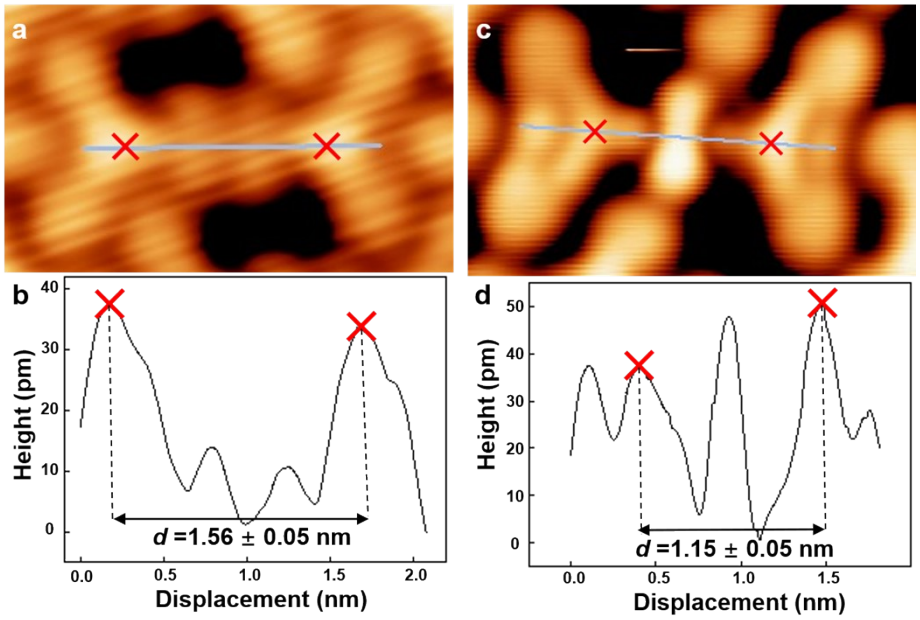


**Figure S5. Profile elevation map of the two dimerization products.** (a) STM image and (b) Profile elevation map of the *d*-dimer, formed via decarboxylative coupling. (c) STM image and (d) corresponding profile elevation map of a short *d*-dimer, formed through a coupling reaction where one HTBA monomer loses a carboxyl group and the other loses a benzoic acid group, followed by C－C bond formation. Tunneling parameters: (a) $V_s = -2.0$ V, $I_t = 100$ pA. (c) $V_s = -1.0$ V, $I_t = 500$ pA.

The distance of the *d*-dimer is measured to be 1.56 ± 0.05 nm, consistent with the theoretical value (1.54 nm), which indicates the decarboxylation dimerization has occurred between HTBA molecules. The distance of the short *d*-dimer is measured to be 1.15 ± 0.05 nm, consistent with the theoretical value (1.11 nm) as shown in Fig. 3c, which will discuss it in detail later.

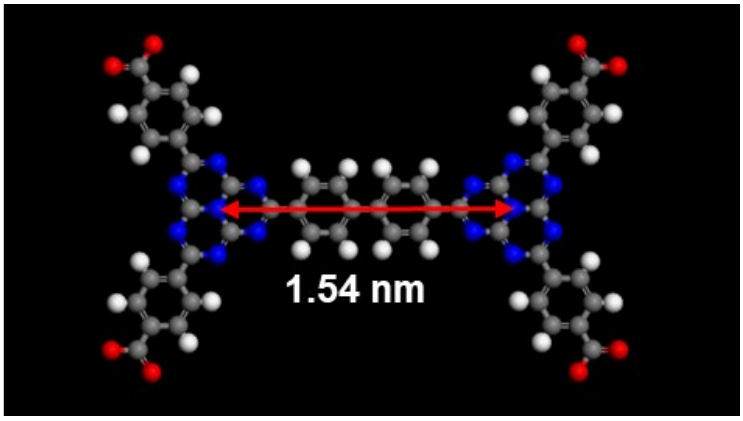


**Figure S6. Structural model of the *d*-dimer.** It indicates the theoretical center-to-center distance between the two reacted HTBA molecules is 1.54 nm.

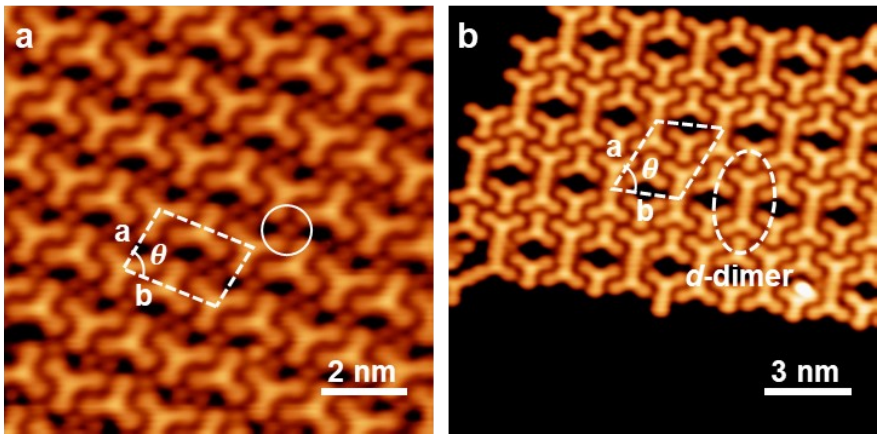


**Figure S7.** STM images of (a) self-assembly and the (b) *d*-dimers with a periodic defect. Tunneling parameters: (a) $V_s$ = − 1.0 V, $I_t$ = 200 pA. (b) $V_s$ = − 2.0 V, $I_t$ = 100 pA.

In addition to the *d*-dimer described above, we also found a *d*-dimer with a periodic defect as illustrated in the Fig. S7a. The molecules within the ribbon continue to assemble in a side-by-side manner, aligning well with the ribbon-like phase mentioned above. However, the molecules between the bands maintain a consistent orientation, all pointing in the same direction and the white circle depicts that Ag adatoms participate in the self-assembly, with the parameters of the unit cell is $\boldsymbol{a}$ = 1.4 ± 0.05 nm, $\boldsymbol{b}$ = 2.2 ± 0.05 nm and $\theta$ = 80° ± 1°. Fig. S7b shows the HTBA molecules undergo dimerization reactions. Interestingly, despite maintaining a periodic structure, each dimer is separated by two unreacted molecules. As a result, each unit cell contains four

molecules in total, with two of them forming a dimer. The parameters of the unit cell are $\boldsymbol{a}$ = 2.3 ± 0.05 nm, $\boldsymbol{b}$ = 2.8 ± 0.05 nm, and $\theta$ = 65° ± 1°. This configuration is likely a consequence of the relative slipping between the ribbon-like phases as depicted in Fig. S7a, driven by thermodynamic forces. Subsequently, dimerization is facilitated by the molecular template effect. X-ray photoelectron spectroscopy (XPS) studies[1] on similar carboxylated species adsorbed on Ag(111) have demonstrated that the O 1s signal associated with the hydroxyl and carbonyl groups diminishes significantly upon thermal annealing in a comparable temperature range which is annealing the sample at ~340 K for ~2 min or kept at RT for a prolonged time (~12 h), while the O 1s signal of carboxylate oxygen appears and maintain a specific proportional relationship with the above two signals, which providing direct spectroscopic signature of dehydrogenation. In addition, the STM evidences[2, 3] previously of the decarboxylation reaction excellent agreement between our structural assignment of the d-dimer and the reported carboxylates on Ag surfaces strongly corroborates our interpretation that the observed transformation is indeed driven by thermally induced decarboxylation.

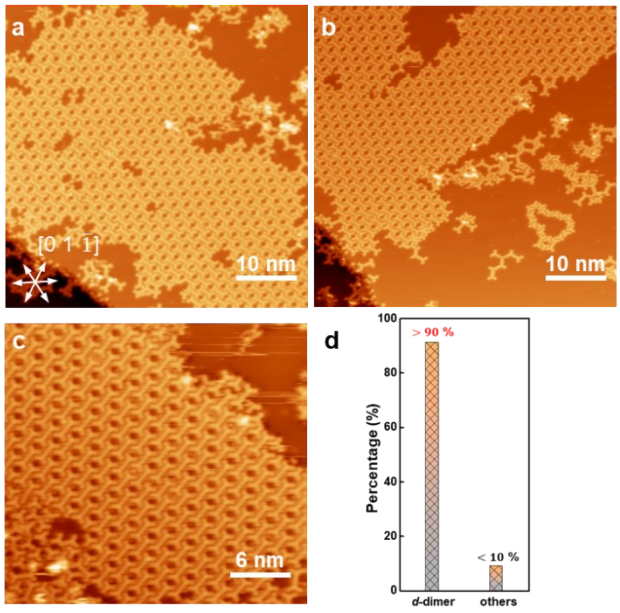

**Figure S8. Selectivity statistics for the *d*-dimer on Ag(111).** (a-c) STM images of the *d*-dimers. (d) Selectivity statistics for the *d*-dimer based on the STM images of (a-c) Tunneling parameters: (a, b) $V_s = -1.6$ V, $I_t = 80$ pA. (c) $V_s = -1.0$ V, $I_t = 110$ pA.

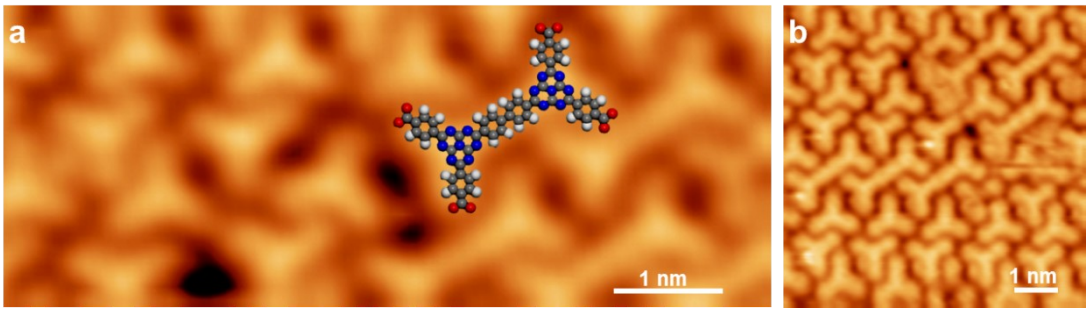


**Figure S9.** STM images of the intermediate state in the domino-like dimerization of HTBA molecules. Tunneling parameters: (a) $V_s = -1.3$ V, $I_t = 290$ pA. (b) $V_s = -1.3$ V, $I_t = 360$ pA.

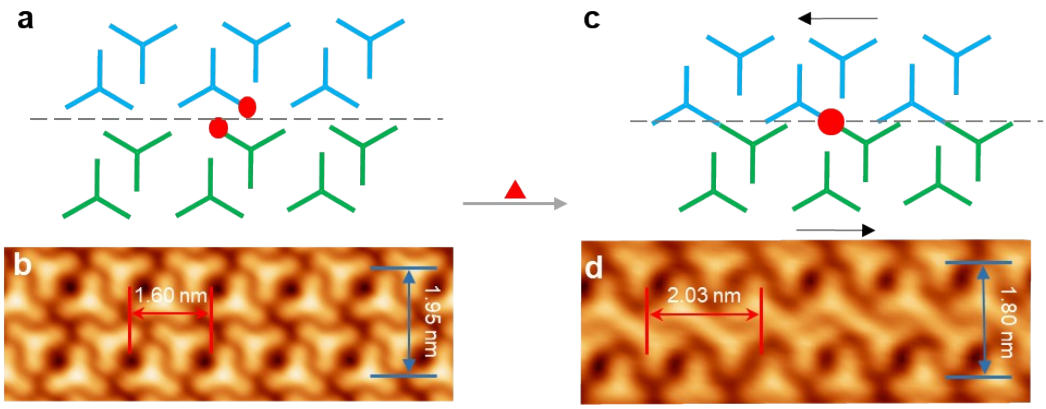


**Figure S10. Schematic illustration of the possible molecular templating mechanism for the selective formation of *d*-dimers.** (a) Molecular model of two adjacent HTBA ribbons (blue and green), with dashed lines indicating the junction of the ribbons where relative displacement occurs. The reactive carboxyl groups relevant to dimerization are highlighted in red. (b) STM image showing the pre-organized ribbon-like suprastructure of HTBA molecules on Ag(111) prior to reaction. (c) Molecular model of two adjacent HTBA ribbons after thermally induced relative displacement. The relative displacement between the two ribbons leads to a head-to-

head alignment of the red-marked carboxyl groups, providing a favorable configuration for coupling. (d) STM image of post-reaction *d*-dimers arranged in a domino-like row. Tunneling parameters: (b) $V_s = -2.0$ V, $I_t = 100$ pA. (d) $V_s = -1.3$ V, $I_t = 300$ pA.

As illustrated in Fig. S10, HTBA molecules are represented by clover-shaped models, with blue and green denoting two distinct molecular ribbon rows. Before the reaction, Fig. S10b clearly shows that HTBA molecules are pre-organized into an ordered ribbon-like suprastructure on the Ag(111) surface. At this stage, steric hindrance causes the three carboxyl reactive sites of each HTBA molecule to be spatially mismatched, preventing direct coupling.[4] Due to thermally induced molecular motion, relative shifts occur between adjacent ribbons. Upon annealing, the molecules can overcome intermolecular interactions and undergo relative displacement between adjacent ribbons along the direction indicated by the dashed lines in Fig. S10a. By identifying the tilt direction of the post-reaction *d*-dimers, we infer that the green ribbons can move relative to the blue ribbons. As shown in Fig. S10c, when the system evolves along this displacement pathway, the two carboxyl groups marked in red in Fig. S10a (the top-left carboxyl group of HTBA molecules in the green ribbon and the bottom-right carboxyl group of HTBA molecules in the blue ribbon) align head-to-head. This geometrically favorable configuration drives the selective decarboxylative coupling,[5] resulting in the formation of a *d*-dimer (Fig. S10d). This inter-ribbon displacement mechanism effectively explains why *d*-dimers tend to appear in aligned chains along inter-ribbon gaps, rather than as isolated dimers. We further propose that *d*-dimer formation follows a domino-like mechanism,[6, 7] propagating unidirectionally along molecular rows. The initial *d*-dimer serves as a driving force, triggering sequential dimerization of neighboring molecules. This hypothesis is supported by our STM observation (Fig. S9) of an arrested intermediate state during the domino process. In addition, we quantified the variation in average intermolecular distance before and after the reaction, a methodological approach previously documented in the literature.[8] We found that the inter-row distance in the Fig. S10 was measured to be 1.95 nm ± 0.05 nm prior to the

reaction, which decreased to 1.80 nm ± 0.05 nm following the reaction, representing a relatively minor change. In contrast, the measured inter-column spacing increased from 1.60 nm to 2.03 nm, which can be attributed to the formation of dimers.

## REFERENCES


1 P. Prochazka, M. A. Gosalvez, L. Kormos, B. de la Torre, A. Gallardo, et al., *ACS Nano*, 2020, **14**, 7269-7279.

2 H.-Y. Gao, P. A. Held, M. Knor, C. Mück-Lichtenfeld, J. Neugebauer, et al., *J. Am. Chem. Soc.*, 2014, **136**, 9658-9663.

3 B. Yang, K. Niu, F. Haag, N. Cao, J. Zhang, et al., *Angew. Chem. Int. Ed.*, 2022, **61**, e202113590.

4 H. Klaasen, L. Liu, X. Meng, P. A. Held, H.-Y. Gao, et al., *Chem. - Eur. J.*, 2018, **24**, 15303-15308.

5 C. Morchutt, J. Bjork, C. Strasser, U. Starke, R. Gutzler, et al., *ACS Nano*, 2016, **10**, 11511-11518.

6 M. Liu, S. Chen, T. Li, J. Wang and D. Zhong, *J. Phys. Chem. C*, 2018, **122**, 24415-24420.

7 C. Ma, J. Wang, H. Ma, R. Yin, X. J. Zhao, et al., *J. Am. Chem. Soc.*, 2023, **145**, 10126-10135.

8 B. Yang, N. Cao, H. Ju, H. Lin, Y. Li, et al., *J. Am. Chem. Soc.*, 2019, **141**, 168-174.